Anthropogenic land use exerts selection pressures on the resistome of a wild rodent

Gicquel, M.[1‡], Planillo, A.[1‡], Heitlinger, E.[1,2,3] , Forslund-Startceva, S.K.[4,5,6], Kramer-Schadt, S.[1,7], Ferreira, S. C. M.[1,2,8], Jarquín-Díaz, V. H.[4,5,6*]

[1]Department of Ecological Dynamics, Leibniz Institute for Zoo and Wildlife Research (IZW), Alfred-Kowalke-Straße 17, 10315, Berlin, Germany.
[2]Institute for Biology. Department of Molecular Parasitology. Humboldt University Berlin (HU). Philippstr. 13, Haus 14, 10115, Berlin, Germany.
[3]Federal State Agency for Consumer & Health Protection Rhineland-Palatinate, Koblenz, Germany
[4]Max-Delbrück-Center for Molecular Medicine in the Helmholtz Association (MDC), Berlin, Germany.
[5]Charité – Universitätsmedizin Berlin, corporate member of Freie Universität Berlin and Humboldt-Universität zu Berlin, Experimental and Clinical Research Center, Lindenberger Weg 80, 13125 Berlin, Germany.
[6]Experimental and Clinical Research Center, a cooperation between the Max-Delbrück-Center for Molecular Medicine in the Helmholtz Association and the Charité - Universitätsmedizin Berlin, Germany.
[7]Institute of Ecology, Technische Universität Berlin, Rothenburgstr. 12, 12165 Berlin, Germany.
[8]University of Veterinary Medicine Vienna, Research Institute of Wildlife Ecology, Veterinärplatz 1 1210, Vienna, Austria

‡shared first authors; *Corresponding author: Víctor Hugo Jarquín-Díaz. Max-Delbrück Center for Molecular Medicine (MDC), Experimental and Clinical Research Center (ECRC) Charité, Campus Buch. Lindenberger Weg 80, 13125, Berlin, Germany.
E-mail: VictorHugo.JarquinDiaz@mdc-berin.de

Supplementary material

Supplementary Table S1. Classification of antimicrobial resistance genes (ARGs) into drug classes and broader drug class groups for the association analysis in the joint species distribution models (jSDMs). To address the sparse representation of certain drug classes, ARGs were grouped into broader drug class groups based on chemical structure and mechanism of action. This table details the reclassification of individual drug classes to their corresponding broader groups, along with the number of ARGs identified per class and per group.

Drug class group	Drug class	Number of ARGs per class	Number of ARGs per group
Aminoglycosides	aminoglycoside	59	59
Aromatics	fluoroquinolone	23	29
	phenicol	3	
	rifamycin	3	
Beta-lactams	beta-lactam	8	39
	carbapenem	4	
	cephalosporin	27	
MLS	elfamycin	7	32
	lincosamide	6	
	macrolide	18	

	streptogramin	1	
Multidrug	multidrug	81	81
Other	aminocoumarin	4	22
	diaminopyrimidine	4	
	mupirocin	1	
	nitroimidazole	1	
	nucleoside	1	
	phosphonic acid	10	
	zoliflodacin	1	
Peptides	glycopeptide	25	48
	peptide	23	
Sulfonamides	sulfonamide	3	3
Terpenoids	fusidane	1	3
	pleuromutilin	2	
Tetracyclines	tetracycline	24	24

Supplementary Table S2. Clinically relevant groups of antimicrobial resistance genes (ARGs).

Gene group	Description	Resistance mechanism	Drug class
CblA	CblA beta-lactamase	antibiotic inactivation	cephalosporin
CepA	CepA beta-lactamase	antibiotic inactivation	cephalosporin
CfxA	CfxA beta-lactamase	antibiotic inactivation	cephamycin
CTX-M	CTX-M beta-lactamase	antibiotic inactivation	cephalosporin
KPC	KPC beta-lactamase	antibiotic inactivation	monobactam, carbapenem, cephalosporin, penam
SHV	SHV beta-lactamase	antibiotic inactivation	carbapenem, cephalosporin, penam
TEM	TEM beta-lactamase	antibiotic inactivation	penam, monobactam, cephalosporin, penem
CfiA	CfiA beta-lactamase	antibiotic inactivation	carbapenem

IMP	IMP beta-lactamase	antibiotic inactivation	carbapenem, cephalosporin, cephamycin, penam
NDM	NDM beta-lactamase	antibiotic inactivation	carbapenem,cephalosporin,cephamycin,penam
VIM	VIM beta-lactamase	antibiotic inactivation	carbapenem, cephalosporin, cephamycin, penam
ACT	ACT beta-lactamase	antibiotic inactivation	carbapenem, cephalosporin, cephamycin, penam
ampC	ampC-type beta-lactamase	antibiotic inactivation	cephalosporin, penam
CMY	CMY beta-lactamase	antibiotic inactivation	cephamycin
OXA	OXA beta-lactamase	antibiotic inactivation	carbapenem, cephalosporin, penam
AAC(3)	AAC(3)	antibiotic inactivation	aminoglycoside
AAC(6')	AAC(6')	antibiotic inactivation	aminoglycoside
ANT(3'')	ANT(3'')	antibiotic inactivation	aminoglycoside
ANT(4')	ANT(4')	antibiotic inactivation	aminoglycoside
ANT(6)	ANT(6)	antibiotic inactivation	aminoglycoside
APH(2'')	APH(2'')	antibiotic inactivation	aminoglycoside
APH(3')	APH(3')	antibiotic inactivation	aminoglycoside
APH(3'')	APH(3'')	antibiotic inactivation	aminoglycoside
APH(6)	APH(6)	antibiotic inactivation	aminoglycoside
vanA	vanA/vanB	antibiotic target alteration	glycopeptide
qnr	Quinolone resistance protein	antibiotic target protection	fluoroquinolone
MCR	Phosphoethanolamine transferase	antibiotic target alteration	peptide
pmr	Phosphoethanolamine transferase	antibiotic target alteration	peptide
Fos	Fosfomycin thiol transferase	antibiotic inactivation	phosphonic acid
cat	Chloramphenicol acetyltransferase	antibiotic inactivation	phenicol

tet	tetracycline-resistant ribosomal protection protein	antibiotic target protection	tetracycline
tet	tetracycline inactivation enzyme	antibiotic inactivation	tetracycline
Cfr	Cfr 23S ribosomal RNA methyltransferase	antibiotic target alteration	oxazolidinone, streptogramin, phenicol, lincosamide
Erm	Erm 23S ribosomal RNA methyltransferase	antibiotic target alteration	macrolide, lincosamide, streptogramin
lnu	Lincosamide nucleotidyltransferase	antibiotic inactivation	lincosamide
Ere	Macrolide esterase	antibiotic inactivation	macrolide
mph	Macrolide phosphotransferase	antibiotic inactivation	macrolide
arr	rifampin ADP-ribosyltransferase	antibiotic inactivation	rifamycin
sul	Sulfonamide resistant	antibiotic target replacement	sulfonamide

Supplementary Table S3. Environmental layers used for modelling ARG occurrence in the mouse gut microbiome. All spatial layers contain continuous data. Year refers to the year of origin of the data. For distance to roads and paths, the references provided refer to the original layers of respective streets and paths used to calculate the distances. Corine Land Cover layer was used to calculate the proportion of agricultural fields (*agri*).

Variable	Environmental layer	Units	Year	Original resolution
agri	CORINE land cover[1]	proportion of agricultural land (land use class 2)	2018	vector data
imperv	Imperviousness [1]	proportion of impervious surface per raster cell	2018	10m raster
tcd	Tree cover density[1]	proportion of area occupied by trees per raster cell	2018	10m raster
swf	Small woody features[1]	proportion of area occupied by linear structures such as hedgerows, as well as patches of woody features per raster cell	2018	100m raster
dist_roads, dist_paths	Distance to roads, distance to paths [2]	streets and paths linear, rasterised and transformed into distances in meters	2018	vector data
catdens, pigdens, poudens	Livestock[3]	Livestock units of cattle, pigs and poultry, transformed into density per hectare	2020	vector data

prec	Precipitation[4]	Monthly total precipitation (l/m2 or mm)	2015-2022	1km raster
temp	Temperature[4]	Monthly average air temperature (1/10 °C)	2015-2022	1km raster

[1] https://land.copernicus.eu/en/products/ (Downloaded 06.02.2024)
[2] obtained from GeoBasis-DE / BKG (2022): https://gdz.bkg.bund.de/index.php/ (Downloaded 07.02.2024)
[3] obtained from the Thünen Atlas: Landwirtschaftliche Nutzung Winterweizen / Landwirtschaftliche genutzte Fläche 2020, https://atlas.thuenen.de/webspace/agraratlas/agraratlas/index.html?LP=2 (Downloaded 18.09.2023)
[4] obtained from the Deutscher Wetterdients: https://opendata.dwd.de (Downloaded 05.11.2024)

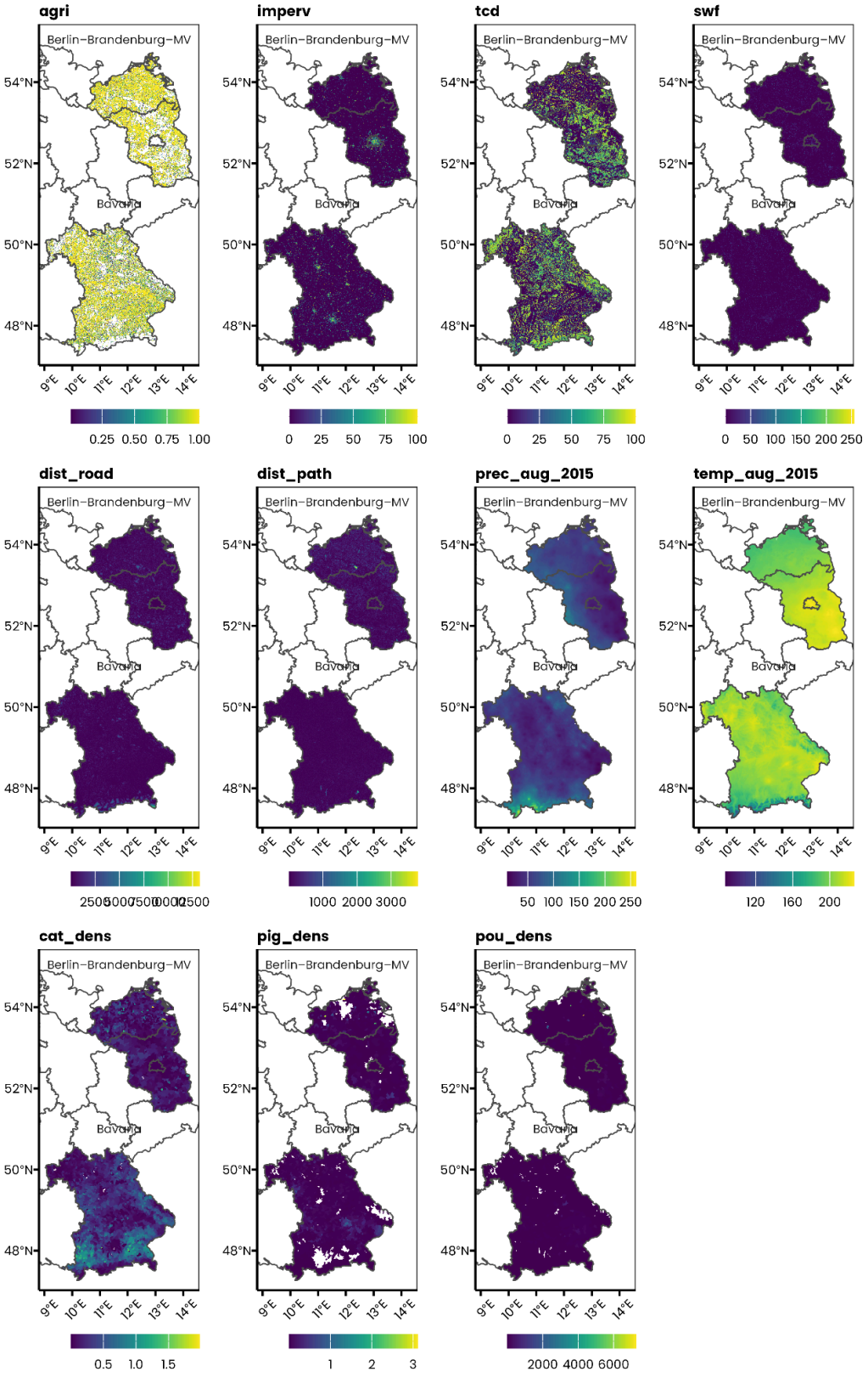

Supplementary Figure S4. Maps of environmental layers in the sampled regions (Berlin-Brandenburg-Mecklenburg-Vorpommern and Bavaria). For precipitation and temperature, we only displayed the values recorded during the year 2015.

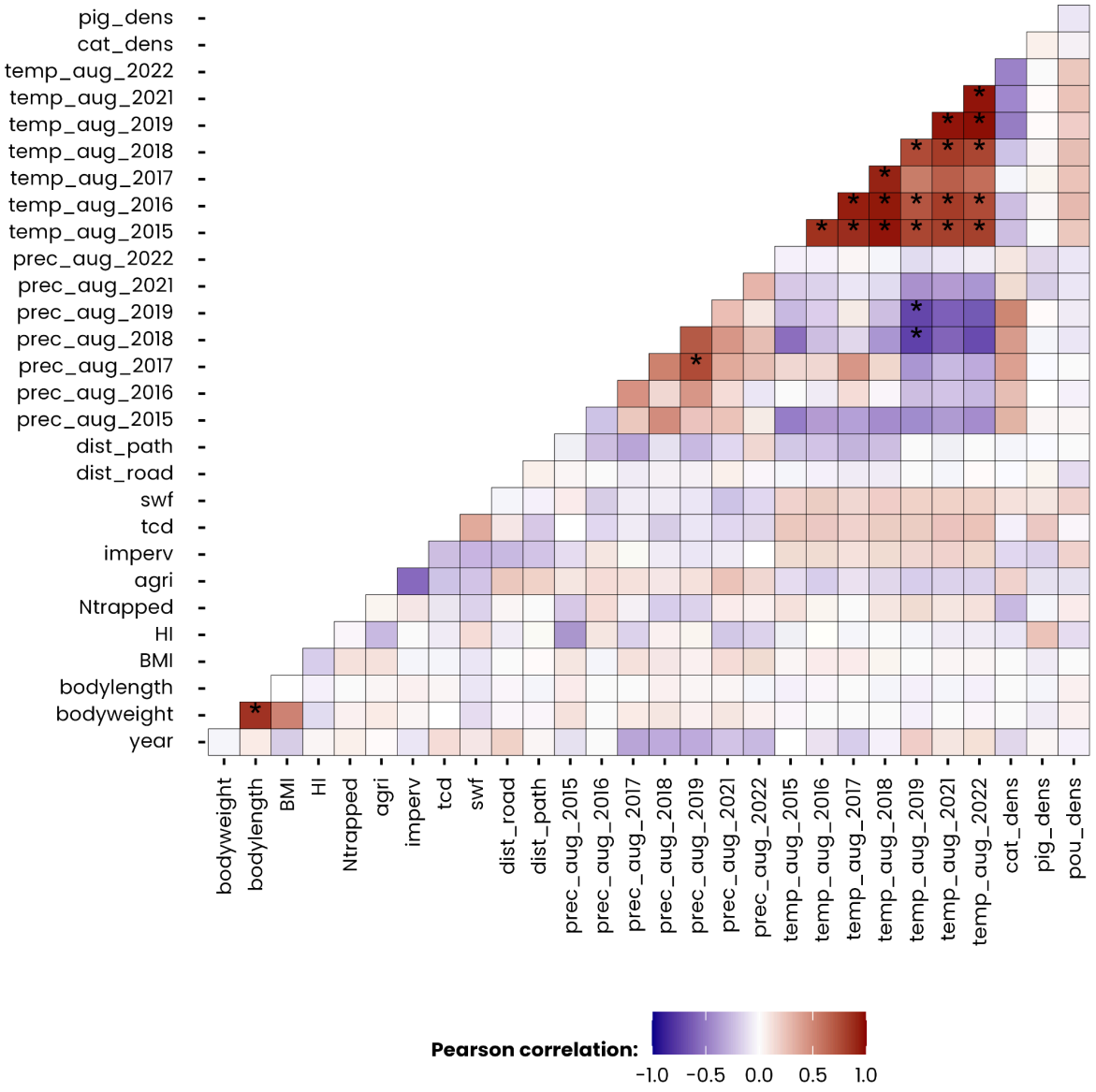

Supplementary Figure S5. Pearson correlation matrix showing the pairwise linear relationships between the explanatory variables. Colours indicate the strength and direction of the correlation, with blue representing negative correlations and red representing positive correlations. Symbol ∗ in tile indicates correlation values |r| > 0.7.

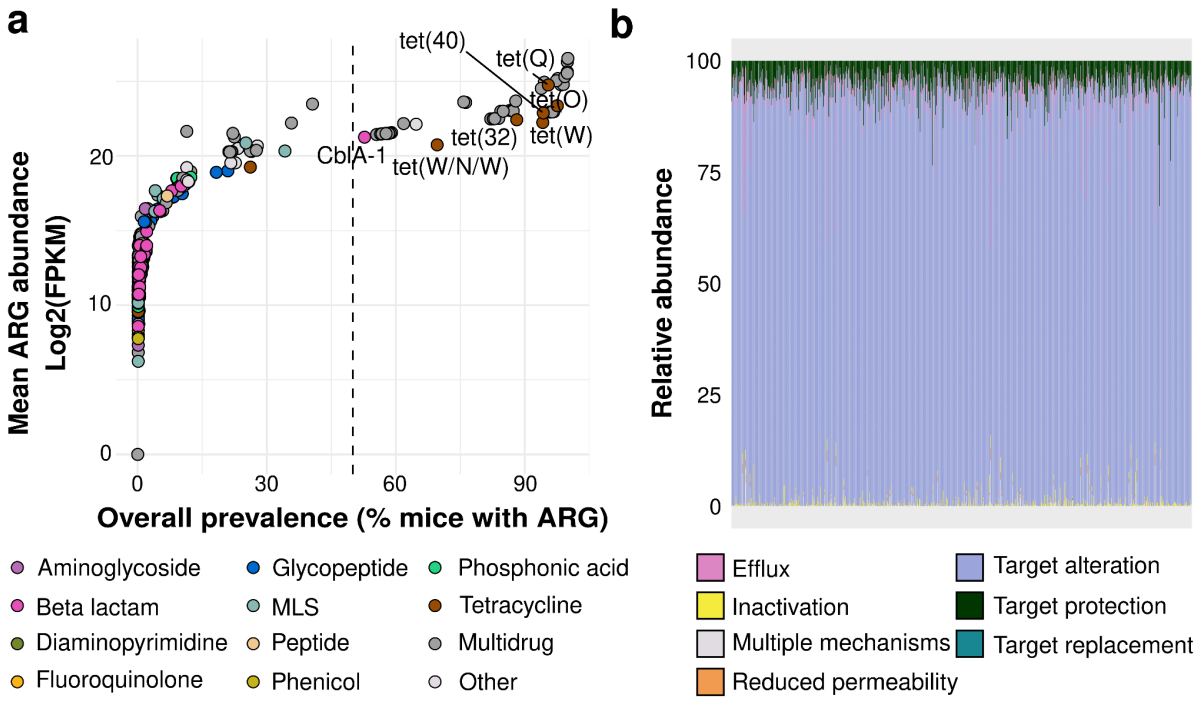

Supplementary Figure S6. Overall prevalence and abundance per ARG. **(a)** Mean abundance and prevalence of ARGs in the colon content metagenomes from house mice. In total, 55 genes had an overall prevalence of more than 50% and a mean abundance over 2,500,000 FPKM across the metagenomes. Only six of these highly prevalent genes confer resistance to two relevant drug classes: tetracycline and beta-lactam. **(b)** Individual mouse relative abundances by resistance mechanism. Genes related to target alteration and protection were consistently more abundant in all mouse metagenomes.

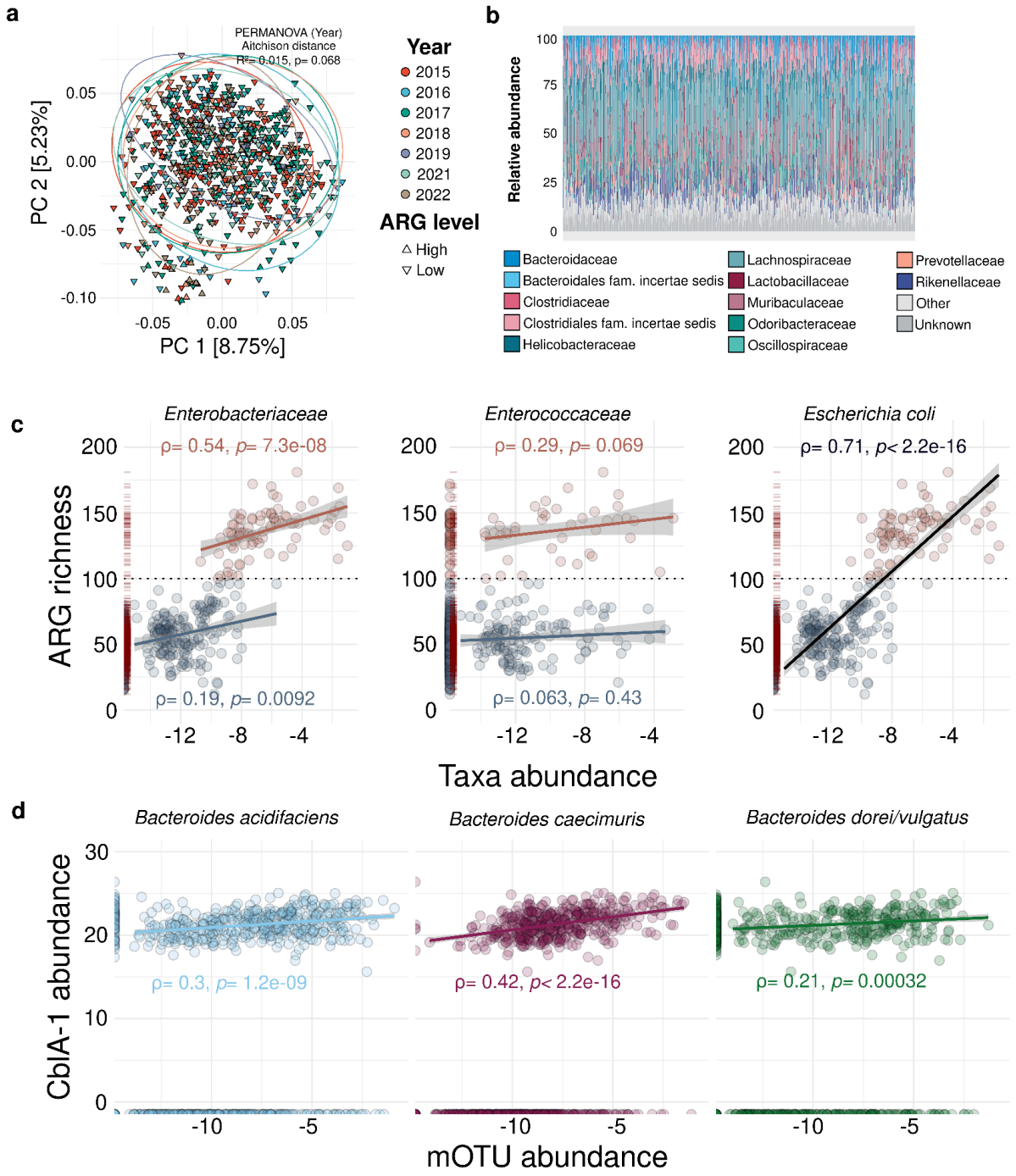

Supplementary Figure S7. General overview of the colon microbiomes from house mice and their relationship to ARG levels. **(a)** Principal component analysis (PCA) showing dissimilarity in microbial composition between years of sampling. Each point represents the colon microbiome of a sample. Distances between points reflect biological gene composition dissimilarity based on Aitchison distances. Points and ellipses are coloured by year of sampling. Shape represents whether an individual metagenome has higher or lower than 100 ARGs predicted. **(b)** Individual mouse relative abundances of operational taxonomic (mOTUs) units agglomerated by bacterial families. mOTUs from the Lachnospiraceae family were consistently more abundant and prevalent in all mouse metagenomes (Mean relative abundance= 25.8% [95%CI: 24.8-26.8], Prevalence= 99.8%). **(c)** Spearman's rank

correlations between microorganisms commonly associated with resistance and ARG richness per mouse. Commensal gut families (*Enterobacteriaceae*, *Enterococcaceae*) explain differences in ARG levels in mice. Higher abundance of such families is related to higher levels of resistance. *Escherichia coli* has a strong correlation to the total ARG richness. **(d)** The abundance of the *CblA-1* gene coding for a Class A beta lactamase is related to *Bacteroides* sp. Within the house mouse microbiome. *B. caecimuris* abundance has a stronger correlation compared to the other two *Bacteroides* species with prevalence above 50%. Taxa abundance is expressed as the log2 of the relative abundance, and for the gene *CblA-1* the abundance is expressed as log2 FPKM.

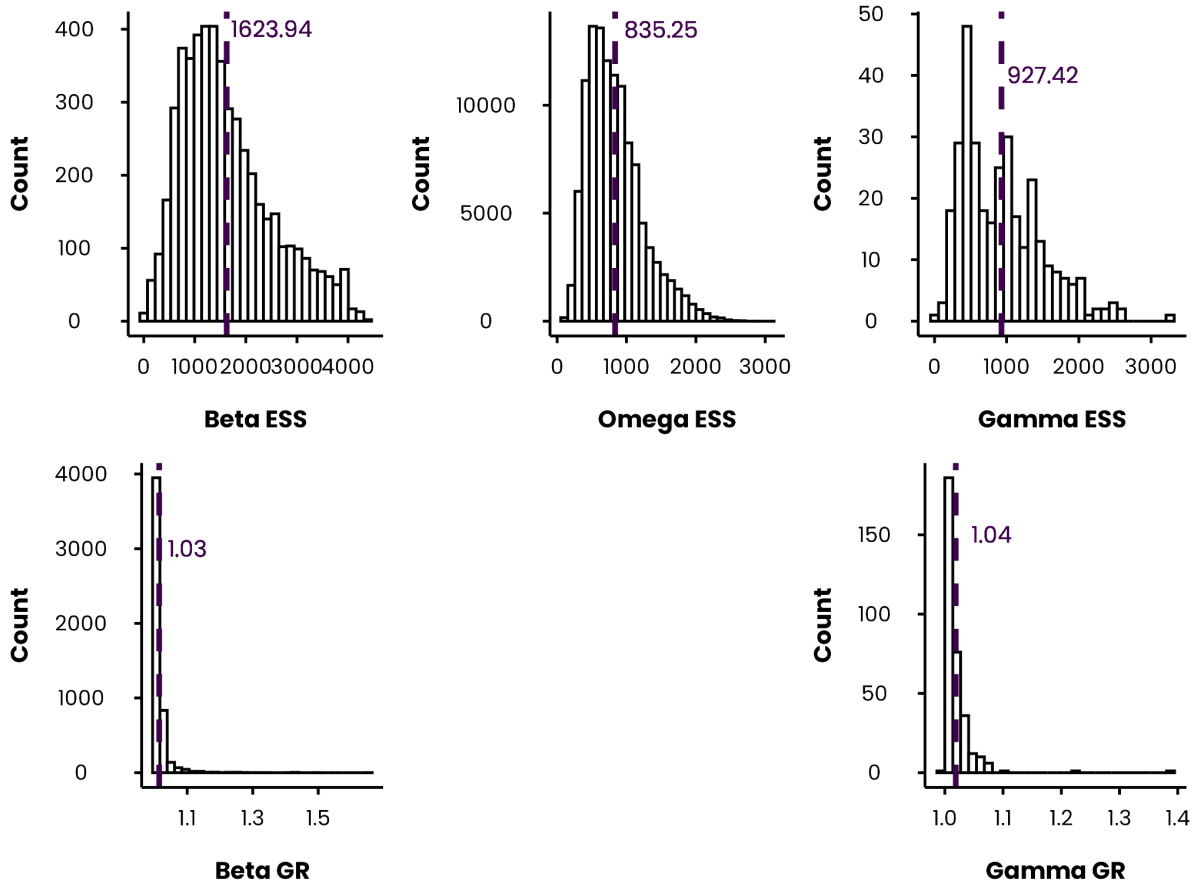

Supplementary Figure S8. Convergence diagnostics for the ARG presence-absence joint species distribution model (jSDM). The top row shows the distribution of effective sample sizes (ESS) for monitored parameters, with the dashed purple line indicating the average ESS. The bottom row shows the distribution of Gelman–Rubin (GR) statistics, with the dashed purple line marking the average GR value. Model convergence: The average effective sample sizes for all parameters are high (>800), indicating that the model estimates robust parameters and exhibits low autocorrelation and good mixing. Gelman-Rubin diagnostic values are acceptable for betas (1.03) and gammas (1.04), which means chains converge well. It could not be compiled for omegas for structural reasons (huge matrices for each sample). Model fit metrics: Pseudo-R^2 (Tjur R^2) = 0.13 , AUC = 0.91, R^2 sp = 0.17, R^2 site = 0.72

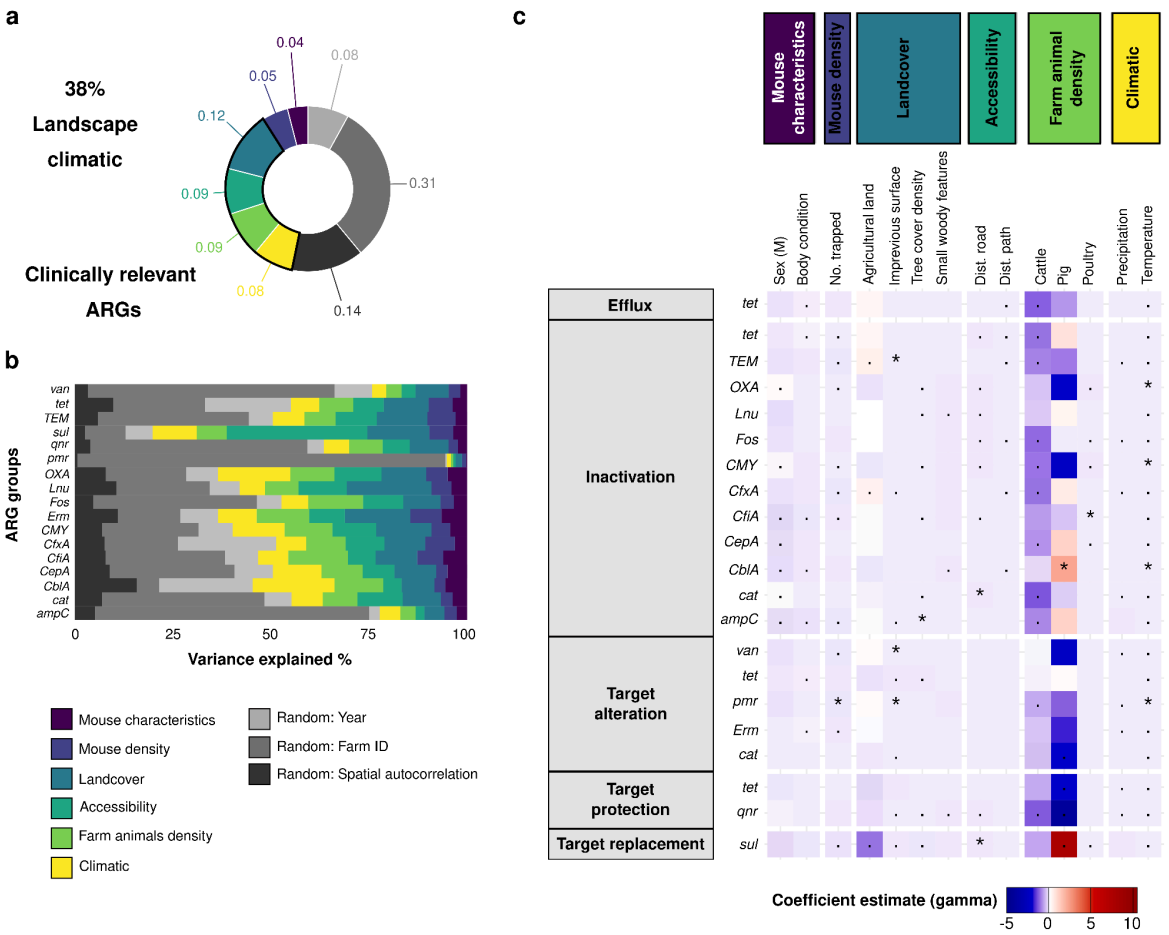

Supplementary Figure S9. Variance partitioning showing the relative contribution of mouse characteristics, environmental factors, and random effects, on the explained variation in clinically relevant ARG occurrence in mouse gut microbiomes. **(a)** Landcover accounts for the higher proportion of variance on these genes **(b)** Variance partitioning in occurrence averaged for each ARG group. For *sul* genes landscape characteristics are particularly relevant and account for more than 70% of occurrence variance. **(c)** The heatmap shows the coefficient estimate (gamma) for each ARG group and a given explanatory variable of the jSDM. Cattle and pig density are explanatory variables with stronger associations compared to other variables in the model. *sul* genes with target replacement mechanism and the *cblA-1* beta-lactamase are strongly and positively associated with pig density ($\gamma > 5$, support: 0.75). *tet* genes are distinctively associated with pig density, while those related to antibiotic inactivation have a positive association, those involved in efflux and target protection mechanisms are negatively associated, and especially the latter with a strong effect ($\gamma < 0$, support: 0.75). The higher the coefficient estimate, the higher the association of the variable with the ARG group. Symbol in tile indicate the posterior probability of the estimate in the model: $*$ > 0.95 and · > 0.75.

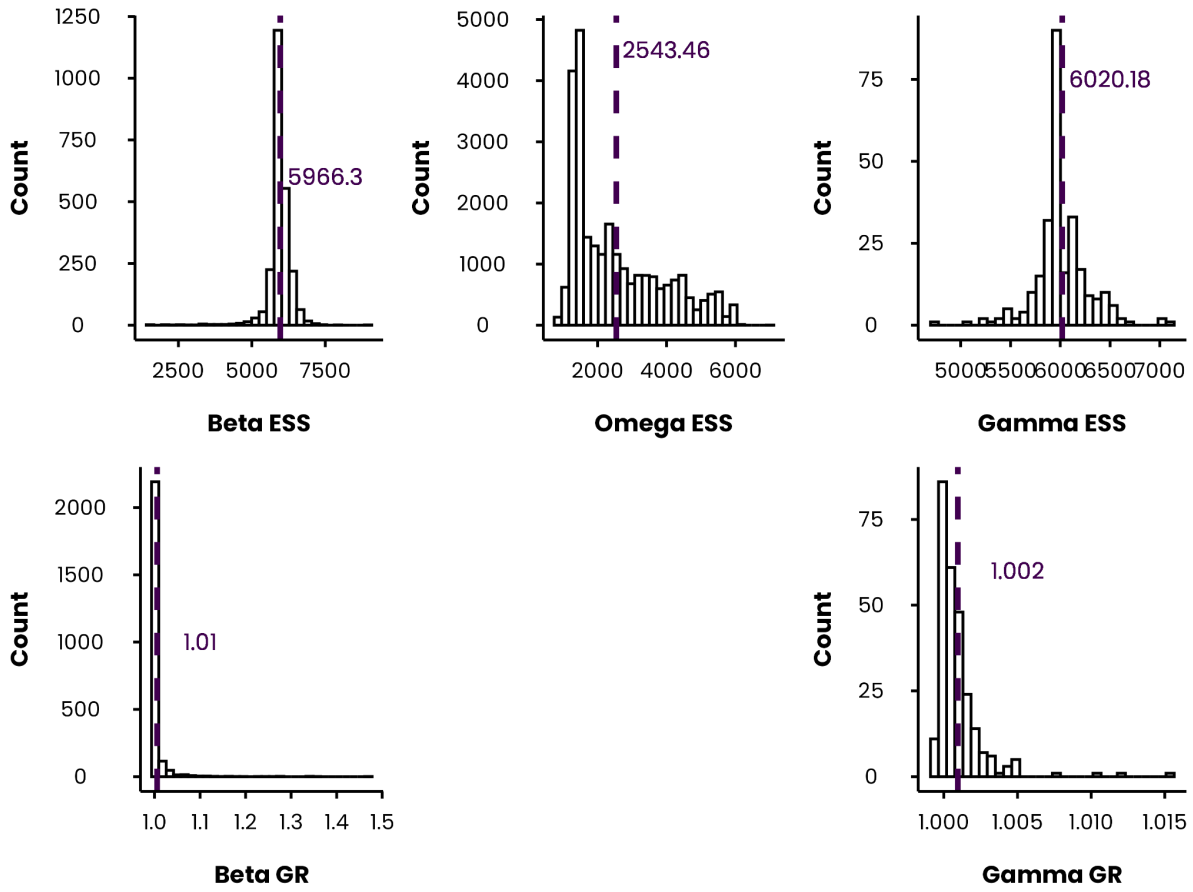

Supplementary Figure S10. Convergence diagnostics for the jSDM ARG abundance model. The top row shows the distribution of effective sample sizes (ESS) for monitored parameters, with the dashed purple line indicating the average ESS. The bottom row shows the distribution of Gelman–Rubin (GR) statistics, with the dashed purple line marking the average GR value. Model convergence: The average effective sample sizes for all parameters are high (>2500), indicating that the model estimates robust parameters and exhibits low autocorrelation and good mixing. Gelman-Rubin diagnostic values are acceptable for betas (1.01) and gammas (1.002), which means chains converge well. Model fit metrics: Pseudo-R^2 (Tjur R^2) = 0.22 , AUC = 0.796, R^2 sp = 0.22, R^2 site = 0.81

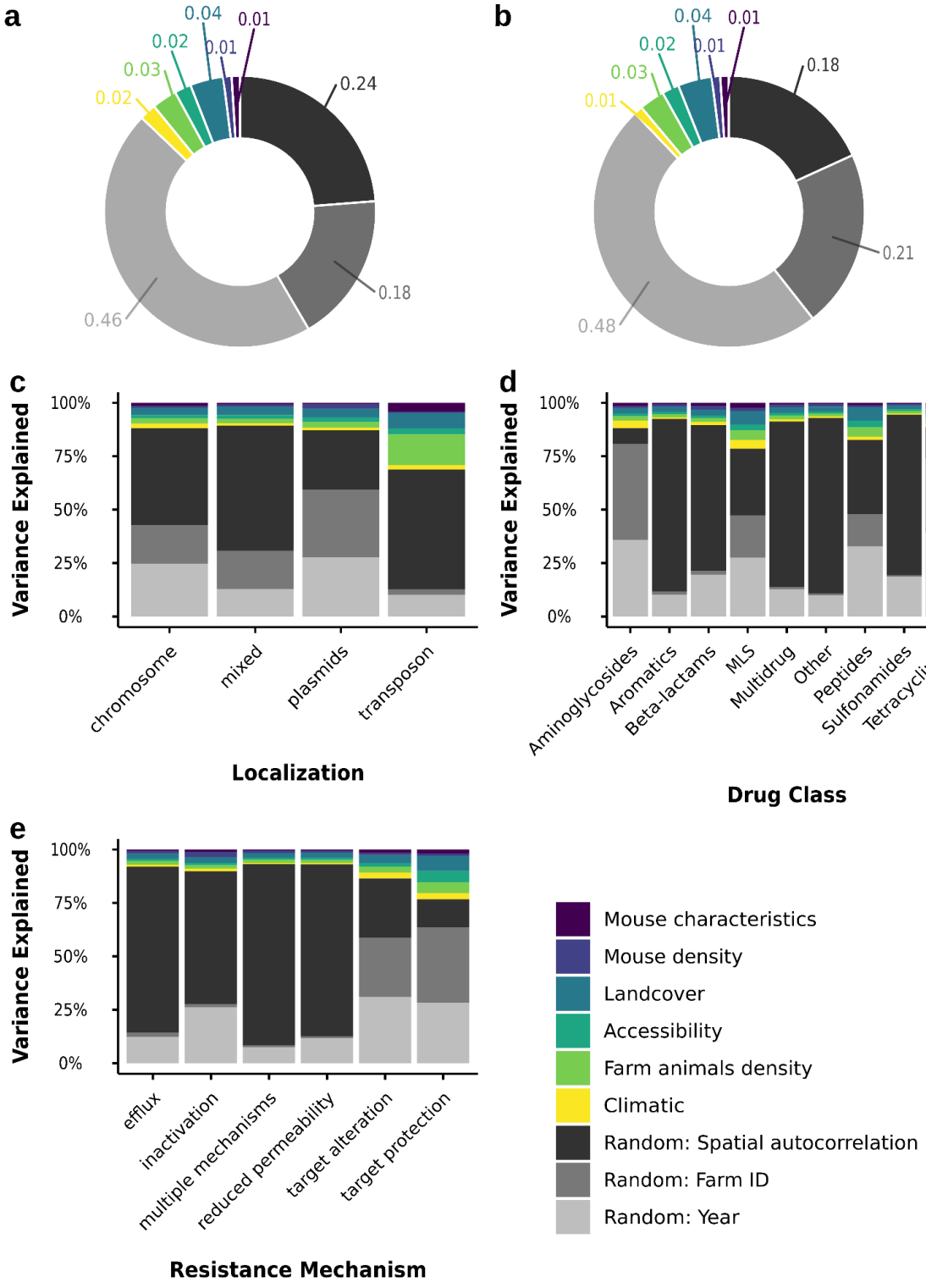

Supplementary Figure S11. Variance partitioning showing the relative contribution of mouse characteristics, environmental factors, and random effects, on the explained variation in ARGs abundance in mouse gut microbiomes **a)** for all genes and **b)** only for mobile genes. **(c-e)** Variance partitioning in abundance averaged for each ARG trait (localization, drug class and resistance mechanism).

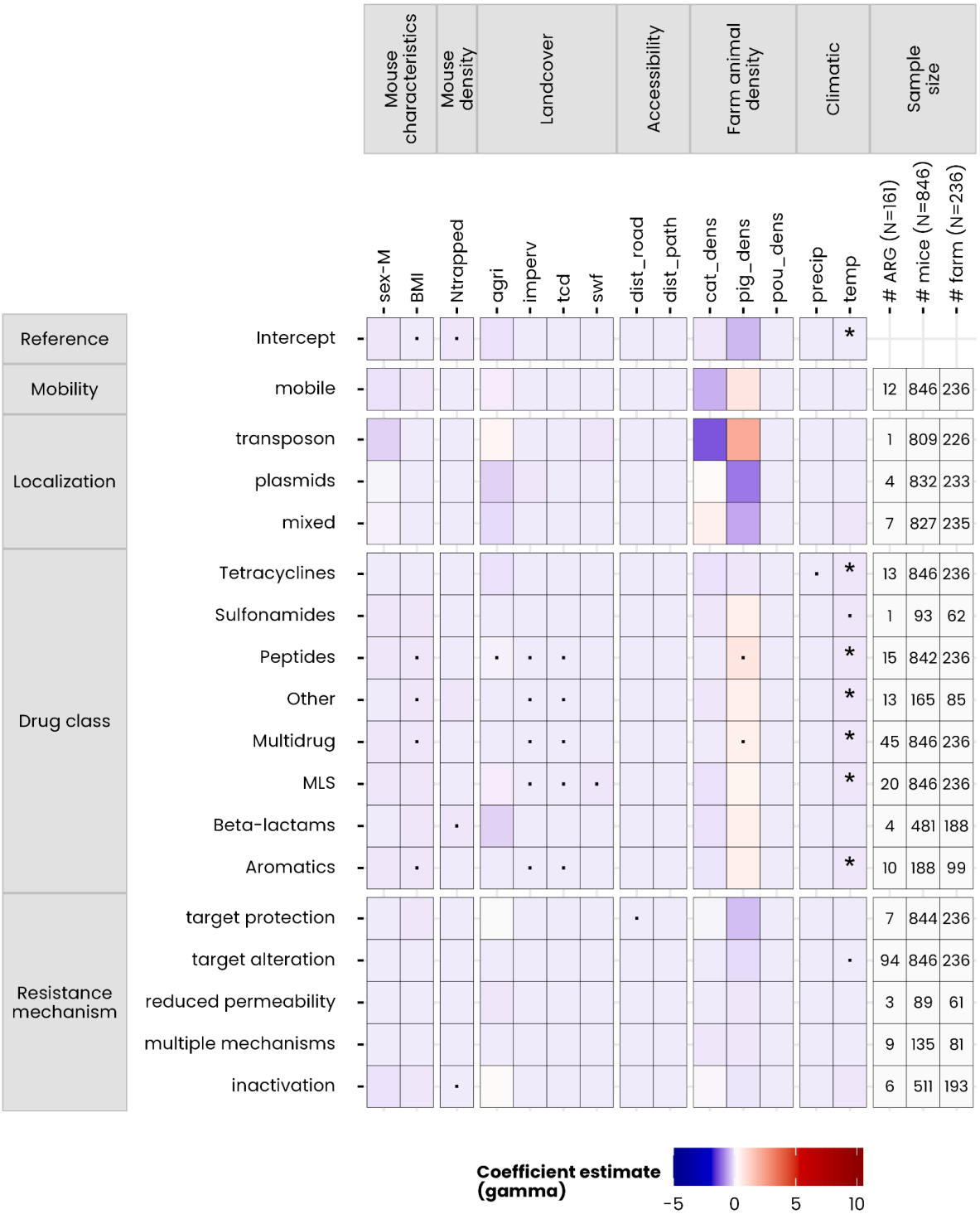

Supplementary Figure S12. Effect of mouse-related, environmental, farm animal density and climatic variables on ARG abundance agglomerated according to their traits. The intercept reference level for traits corresponds to ARGs that are non-mobile, located on chromosomes, giving resistance towards the aminoglycoside drug class, and having an efflux resistance mechanism. Symbol in tile indicate the posterior probability of the estimate in the model: ∗ > 0.95 and · > 0.75.

Supplementary Table S13. Differences in ARG richness between house mice and livestock manure

Host 1	Host 2	P-value adj.	Significance	Effect size	Contrast
House mice (n=859)	Cattle (n=29)	4.73E-19	****	0.31	306±16.4
	Chicken (n=238)	1.29E-121	****	0.71	416±6.4
	Pig (n=269)	6.10E-132	****	0.73	173±6.1
	Turkey (n=17)	1.56E-12	****	0.24	497±21.2